ELSEVIER

Thermochimica Acta 332 (1999) 125–142

thermochimica acta

Structure correlated properties of metallocene catalysed polyethylenes by modulated temperature differential scanning calorimetry

J.J. Janimak*, G.C. Stevens

Department of Chemistry, Polymer Research Centre, University of Surrey, Guildford GU2 5XH, UK

Abstract

Conventional and modulated temperature differential scanning calorimetry (MT-DSC) have been used to evaluate quantitatively the thermal properties of a set of advanced polyethylenes synthesised from metallocene catalysts. This study is sought to establish correlations between polymer chain molecular characteristics and crystallisation behaviour in a set of tailor-made polyethylenes.

Melting is described by at least two different structure forming processes that behave independently of each other with Avrami analysis showing singular exponents and low rate constants from melting kinetic data. Avrami exponents from crystallisation kinetic data are broadly in line with typical values for polyethylene. Non-isothermal crystallisation kinetic studies revealed the presence of dual crystallisation peaks on linear cooling from the melt. The first crystallisation peak was found to shift moderately with cooling rate to lower temperatures of crystallisation whereas the second crystallisation peak remained invariant.

Application of MT-DSC following discrete step-wise crystallisation has been successful at identifying initial crystallinities and the presence of reorganisational crystallisation during polymer melting. Melting is seen primarily in the reversing signal of the modulated heat flow, and reorganisational crystallisation during melting in the non-reversing heat flow signal.

Keywords: Crystallisation; Kinetics; Melting; MT-DSC; Polyethylene

1. Introduction

Metallocene catalysed polyethylenes of known density, molecular weight distribution and characteristics (viz., monomodal, bimodal and distributed molecular weight distributions) with variable comonomer and short-chain branch contents were used in this study. DSC and MT-DSC work using well-defined thermal programmes to determine melting/crystallisation and fractional crystallisation was undertaken. In parallel with these studies a series of isothermal and non-isothermal crystallisation experiments were carried out on pre-screened materials. The results of these experiments were analysed by well-established analytical methods to characterise the crystallisation behaviour, crystallisation rate and geometry of developing crystallites.

Typically, polymer crystals are small compared to most inorganic crystals and are by and large quasi-stable [1]. They tend to exhibit a continuous distribution of non-equilibrium melting points owing in part to a distribution of lamellar thicknesses and molecular weights present within

*Corresponding author.

0040-6031/99/$ – see front matter
PII: S0040-6031(99)00067-2

diverse and defected microstructures that describe the overall polymer morphology [2]. Successive melting of the crystallite population is the primary cause of the characteristic feature of a broad melting point on heating. Usually, this range is typically 40–80 K on heating, whereas on cooling the detectable crystallisation range could be as narrow as a few tens of degrees [3].

In this work, we explore the utilisation of bulk crystallisation kinetics via quasi-isothermal crystallisation experiments in a series of metallocene catalysed polyethylenes which exhibit potential molecular segregation effects. These measurements provide new insights into recrystallisation and re-organisation events during melting. Crystallisation from the melt in these metallocene polyethylenes is very rapid and is not easily followed in the DSC. Consequently, the bulk crystallisation kinetics were obtained from crystallinities measured by melting experiments following isothermal crystallisation at a number of different temperatures. In exploring the extent to which fractional crystallisation plays an important role, the maximum melting temperature from quasi-isothermal step-wise experiments was determined. This showed little increase in melting temperature in comparison with measurements from linear heating ramps at low scan rates in conventional DSC. The thermal behaviour of the materials examined here is remarkably similar despite their very different molecular characteristics.

2. Experimental

All measurements were performed on a TA Instruments 2920 DSC equipped with liquid nitrogen assisted cooling. This instrument was operated as a conventional heat flux DSC and as a modulated temperature DSC (MT-DSC). Temperature calibrations were made using high purity standards; benzoic acid, indium, tin, lead and zinc at a scan rate of 10°C/min. Calibration for heat flow scales was done using indium as reference and checked via heat capacity measurements with a sapphire disc in the range of interest. Temperature correction on cooling was performed using indium of various masses at different cooling rates and extrapolated to zero scan rates. Sample masses and reference pans were determined to the nearest μg. An Intel Pentium 166 MHz PC was used to collect and analyse the DSC thermograms.

Our ethylene/1-hexene random copolymers with known branch content, molecular weight and polydispersity were kindly provided by Fina Research (Belgium) through the Fina-Surrey Scholar research programme. Details of as-received materials are listed in Table 1.

2.1. Isothermal crystallisation kinetics

Isothermal crystallisation kinetic experiments were performed using two DSC instruments. A TA Instru-

Table 1
Molecular and melting characteristics of as-received material

Reference	Units	Polymer A	Polymer B	Polymer C
Catalyst type		Cr [a]	Met [b]	Met [b]
Density		0.934	0.922	0.927
Mn	kDa	17	25.8	37.9
Mw	kDa	223	172	83
Mz	kDa	2303	734	147
Mw/Mn		13.2	6.7	2.2
SCB(/1000C) [c]		6.8	9.7	4.3
T_m	°C	123.3	116.1	122.4
ΔH_m (10°C/min)	J/g	128.4	123.9	139.0
$\omega^{c\,d}$	%	44	42	47

[a] Chromium catalyst.
[b] Metallocene catalyst.
[c] Short chain branching (butyl branches) via C^{13} NMR.
[d] Weight fraction crystallinity.

ments 2910 DSC was used to heat specimens to 80°C above their observed melting temperature at a scan rate of 10°C/min where they remained for a period of 3 min under strong nitrogen purge. They were then transferred immediately in air to a 2920 MDSC, which was held at an isothermal temperature (in the range 90–123°C). During the transfer the temperature of the sample pan decreased by several degrees but the initial temperature in the 2920 DSC was still well above the crystallisation temperature range and the highest measured melting point; equilibrium was established in the 2920 DSC within 20 s.

A second crystallisation procedure involved cooling specimens from the melt at 200°C in the 2920 DSC to a temperature just above the observed maximum melting temperature. This was followed by quenching to the desired crystallisation temperature. This latter technique was frequently used to avoid undercooling effects commonly observed in traditional thermal programs. In both cases, the resulting crystallisation exotherm was recorded. Similarly, parallel experiments aimed at evaluating the melting kinetics were performed; here specimens were allowed to crystallise for specific lengths of time and then heated without cooling to above their melting temperature at a scan rate of 10°C/min. The nitrogen gas purge rate was 40 ml/min and sample masses were approximately 3–5 mg. The crystallisation temperature range was from 90–123°C and data were analysed using conventional Avrami analysis. Both sets of data arising from crystallisation and melting were analysed by determining the heats of crystallisation and fusion and in the case of melting kinetics by deconvoluting the contributions to the melting peaks.

2.2. Non-isothermal crystallisation kinetics

Specimens were heated at 10°C/min to 80°C above their observed melting temperature where they remained for 3 min before being cooled at specific rates under an imposed linear temperature program. The range of cooling rates examined varied from 80°C/min to 1°C/min. All specimens were cooled to below room temperature and reheated at 10°C/min to above their melting temperature. All experiments were carried out under a dry nitrogen purge of 40 ml/min. Sample masses were no greater than 5 mg.

2.3. Determination of crystallinity

Crystallinity measurements were performed by integrating under the heat flow curves of either the melt or the recrystallisation transitions. Heat flow scales were normalised with respect to sample mass and compared with literature standard heat of fusion values for polyethylene, 293 J/g was used to represent 100% degree of crystallinity [4].

3. Results

3.1. Thermal characterisation

Fig. 1 shows comparative melting traces of chromium versus metallocene catalysed medium density polyethylenes. The molecular characteristics and initial thermal properties of these polymers are tabulated in Table 1. In analysing the melting curves, we elected to integrate the melt region form a point where the underlying baseline started to deviate at room temperature to its return 20°C above the main melting transition. Melting points were assessed by measuring the peak melting temperatures of near Gaussian shaped melting trace endotherms since peak-widths at half-height were always nearly in excess of 5°C. It is known that the DSC sample-cell response function has an influence on the lineshape of polymer crystal melting. We utilised simple Gaussian line profiles in our peak fitting algorithms as a convenient tool in estimating the potential spectrum of melting.

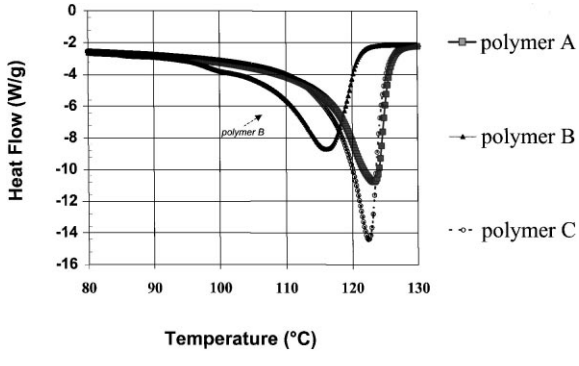

Fig. 1. Melting endotherms of as-received medium density polyethylene pellets.

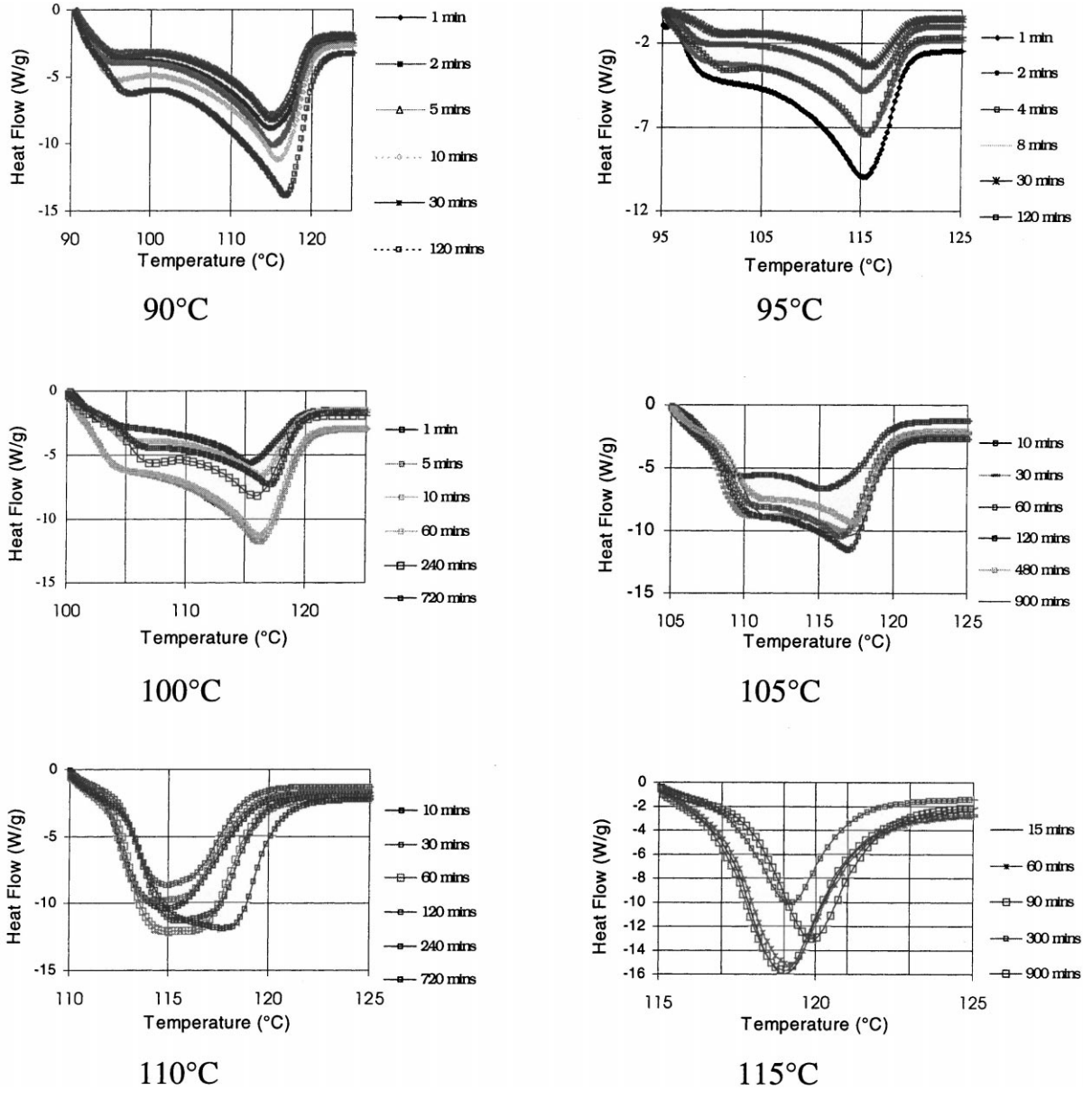

Fig. 2. DSC melting curves for polymer B crystallised isothermally from 95°C to 115°C. Note shape change in melting profile from low temperature melting to melting characteristics at the highest temperature region.

3.2. Melting kinetics

Fig. 2 shows melting traces generated from isothermal crystallisation experiments at specific temperatures for one metallocene polyethylene (polymer B). The melting traces of polymer B following crystallisation at 90°C produced a broad melting endotherm with peak-widths at half-height varying anywhere from 7.9°C to 8.4°C. This result is replicated at 115°C with one main distinct melting peak and a tighter distribution of peak-widths at half-height that varied anywhere from 2.3°C to 2.6°C depending upon

duration of crystallisation. The development of a second melting peak was observed between these two temperatures. The lower of the two melting peaks increased in enthalpy and merged with the upper melting peak at a temperature of 115°C, the highest temperature we examined.

Fig. 3 shows a collection of deconvoluted melting endotherms taken at different crystallisation temperatures for this polymer. Deconvolution was achieved using Gaussian peak fitting algorithms to separate overlapping peak areas. Results show that in most cases at least two Gaussian peak fits are required to describe the melting region. An extreme example is highlighted in Fig. 3(a) at 90°C where five Gaussian peak fits were required to accurately represent the area under the curve. In contrast to this, crystallisation at 115°C represented by Fig. 3(d) produced a sharp melting peak that was close to a Gaussian lineshape. We believe that the asymmetry arises directly from the underlying response function of a scanning calorimeter. This effect is most marked at the upper end of a melting peak.

3.3. Crystallisation kinetics

Fig. 4(a) and (b) shows the crystallisation exotherm of polymer B at 110°C and polymer C at 115°C, respectively. In these examples, the samples were cooled from just above the observed melting temperature to the appropriate crystallisation temperature. In either case, a high temperature conditioning cycle at 200°C in the melt preceded crystallisation to ensure that existing crystal-nuclei were removed. In Fig. 4(a), the peak in the curve occurs approximately 40 s after attaining quasi-equilibrium conditions (total heat flow nearly equal to zero) with all primary crystallisation processes complete after 10 min. The onset of crystallisation occurred immediately on reaching the isothermal crystallisation temperature, hence, no correction for an induction period was necessary. Small exothermic fluctuations appear to the right of the main peak which are related to small temperature variations following the main crystallisation process. The total crystallinity was measured from the integral of all the exothermic peaks and found to be 20%. This value compares favourably via the heat of fusion value obtained on immediately heating the sample (also 20%). From Fig. 4(b), the crystallisation behaviour is slightly different with two crystallisation exotherms that have their maximum after 40 and 80 s from the onset of crystallisation. A small delay prior to crystallisation was observed in Fig. 4(b), which can be attributed to the thermal inertia involved in going from 125°C to 115°C. The measured crystallinity was approximately 33% in this case.

3.4. Avrami analysis

In describing the overall crystallisation kinetics, Avrami analysis was applied to quantify crystallisation rate constants and define the types of crystallite geometries generated by crystallisation [5]. The crystallisation kinetics can be followed through discrete partial integration of the area under the crystallisation curve, normalised by the total area under the curve. The Avrami expression (Eq. (1)) can be cast in its most familiar form of

$$\Delta H_f(t)/\Delta H_f(\text{tot}) = 1 - \exp(-kt^n), \qquad (1)$$

where $\Delta H_f(t)$ is the heat evolved at time t and $\Delta H_f(\text{tot})$ is the total heat evolved during complete crystallisation. $\Delta H_f(t)/\Delta H_f(\text{tot})$ is a measurement of actual crystal transformation at a particular crystallisation temperature, k is the rate constant, t, the time of crystallisation, and n the Avrami exponent.

Fig. 5 shows the analysis following standard Avrami treatment of polymers B and C under isothermal crystallisation conditions at 110°C and 115°C, respectively. The top set of data corresponding to polymer B shows crystallisation kinetics normalised to 58 J/g which corresponds to an absolute weight fraction crystallinity of 20%. The bottom set corresponding to polymer C shows crystallisation kinetics normalised to 98 J/g which corresponds to 33% crystallinity.

For polymer C there was a local minimum at approximately 60 s crystallisation time (area marked on figure by arrows pointing up and down) corresponding to the valley between the two maxima in Fig. 4(b). Using least squares fitting, two distinct structural development processes could be seen taking place. The first, which ends after approximately 40 s crystallisation is immediately followed by a second process that takes place over a longer period of time. An equation of best fit that describes the overall crystallinity development in polymer C was applied

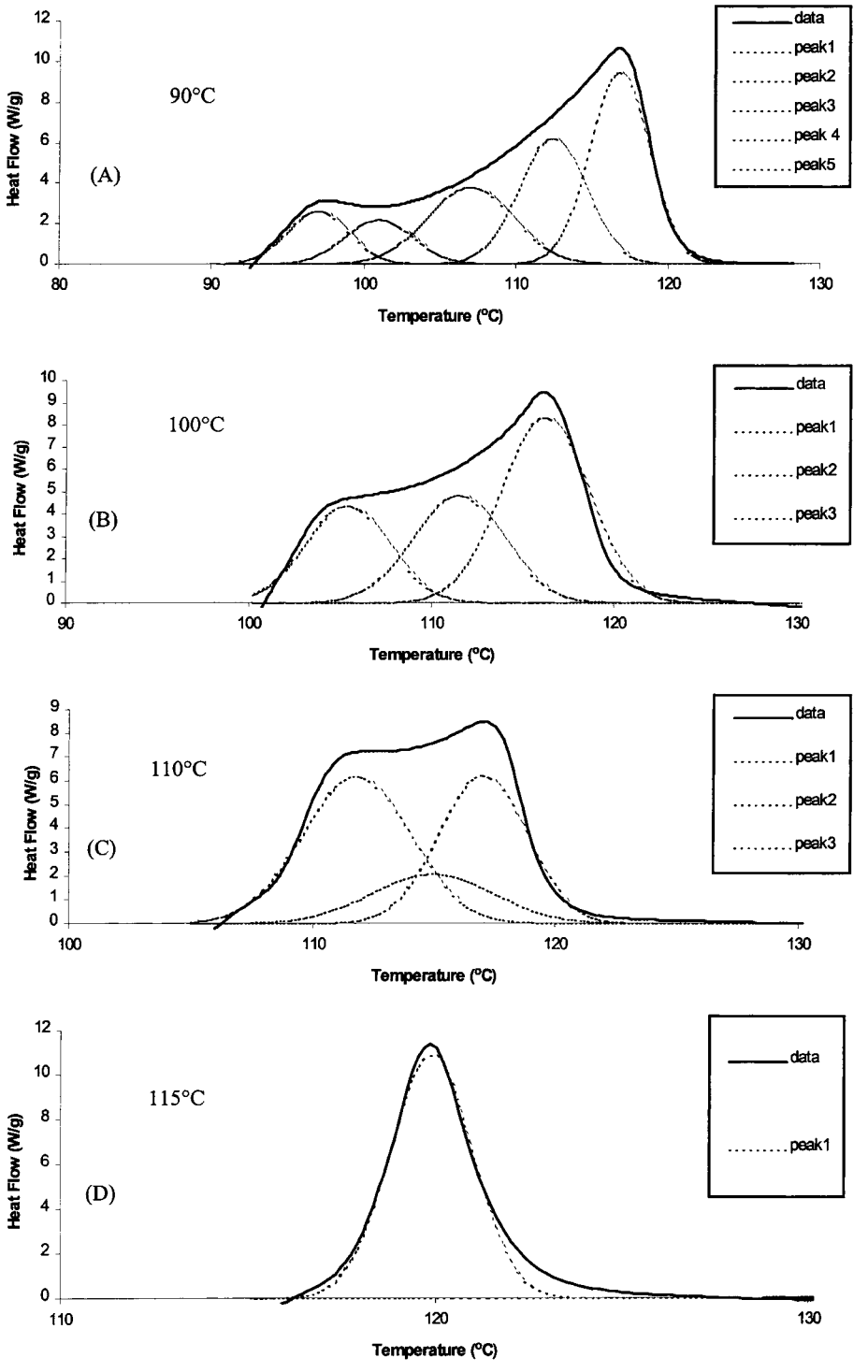

Fig. 3. Deconvoluted melting endotherms after crystallisation at the temperatures shown (polymer B). A Gaussian peak-fitting algorithm was applied to describe the area underneath the curve.

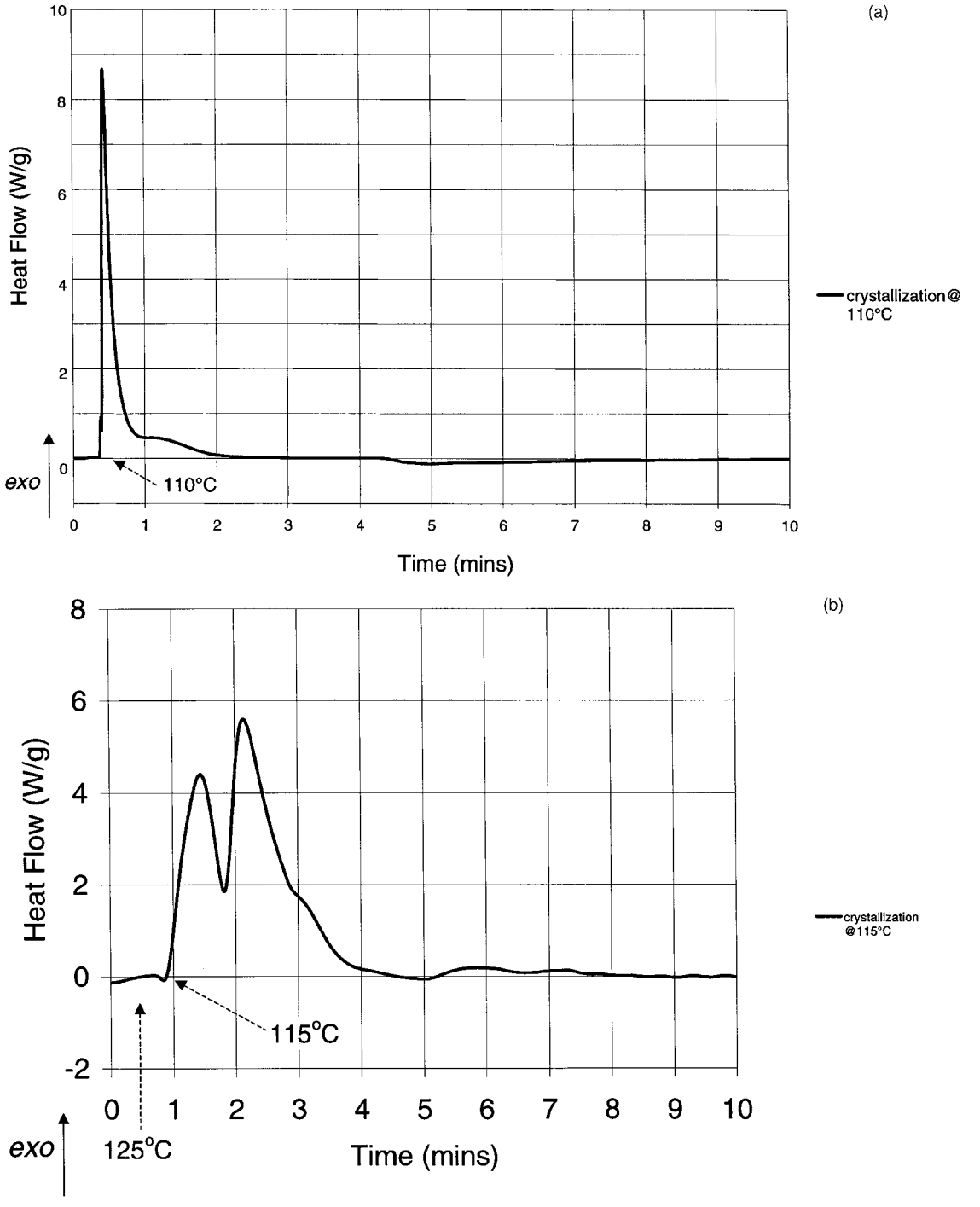

Fig. 4. Crystallisation exotherm of (a) polymer B at 110°C. T_{max} occurs after 40 s crystallisation and complete crystallisation was attained after 10 min. The heat of fusion was estimated to be 58 J/g corresponding to approximately 20% crystallinity; (b) polymer C at 115°C. Local minimum in growth rate found after 60 s crystallisation with complete crystallisation occurring shortly thereafter. The heat of fusion was estimated to be 98 J/g corresponding to approximately 33% crystallinity.

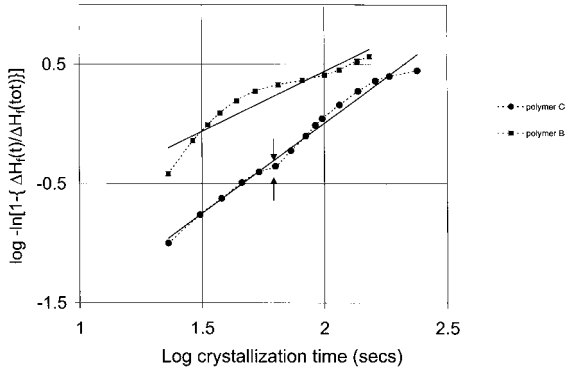

Fig. 5. Avrami plots (log $-\ln[1-\{\Delta H_f(t)/\Delta H_f(\text{tot})\}]$ versus logarithm of crystallisation time) for polymers B and C using the data of Fig. 4(a) and (b). The straight lines through the data set represents the best lines of fit using the method of least squares (see text).

to the Avrami data. The line of best fit is $y=1.52x-3.02$ and is represented by the continuous line. For polymer B, where the least squares fit to the Avrami treated data is poor, the continuous line is given by $y=1.00x-1.60$. In this case, after approximately 40 s crystallisation only then is a large part of the primary crystallisation process complete with slower structural changes extending to longer times. The slopes of these curves (Avrami exponents), which describes the geometry of growth and the intercepts that measure the rate constants are very different. Polymer C has the larger Avrami exponent with pseudo crystallite sizes, ($n\sim1.5$), and polymer B low dimensional developed growth ($n\sim1$). Despite having a low rate constant, polymer B reaches terminal crystallinity at a much earlier stage than polymer C whose development progresses steadily with time.

Fig. 6 shows Avrami kinetics generated from melting data for polymer B at different isothermal crystallisation temperatures. The bold lines through the data set represent the best lines of fit. Low Avrami exponents (less than 1) were observed with rate constants that closely resembled those seen for the secondary

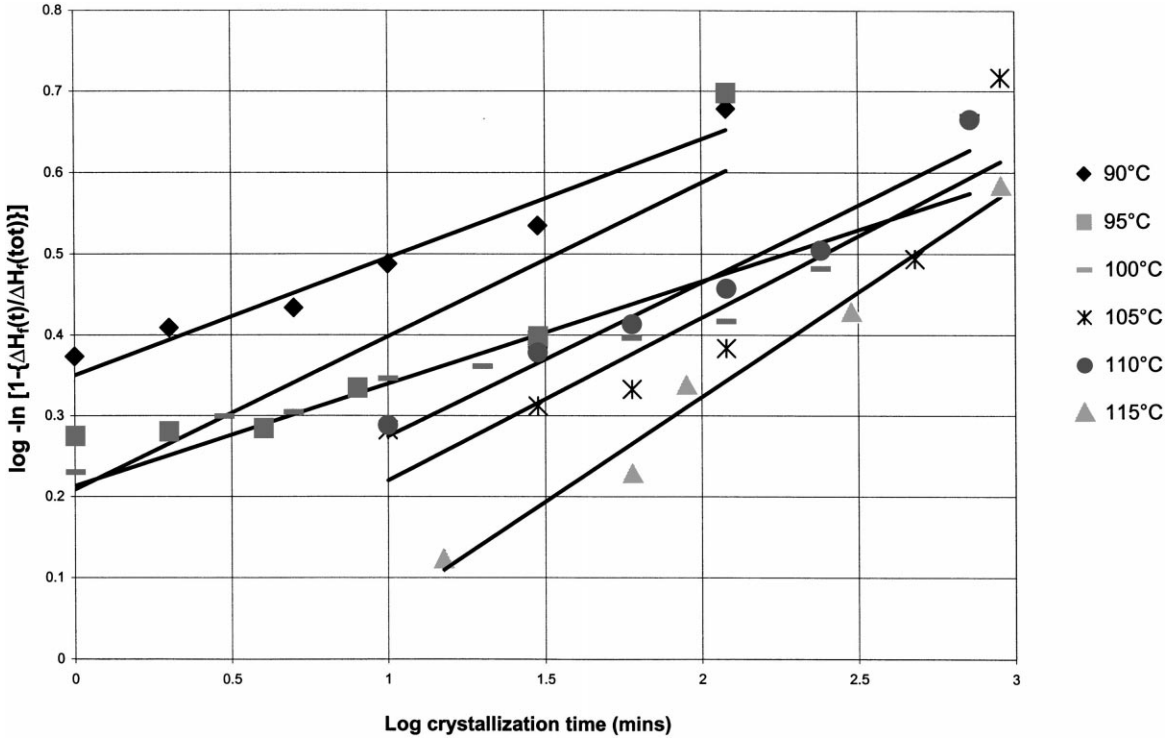

Fig. 6. Avrami plots (log $-\ln[1-\{\Delta H_f(t)/\Delta H_f(\text{tot})\}]$ versus logarithm of crystallisation time) for polymer B using the data of Fig. 2. The straight lines through the data set represents the best lines of fit using the method of least squares.

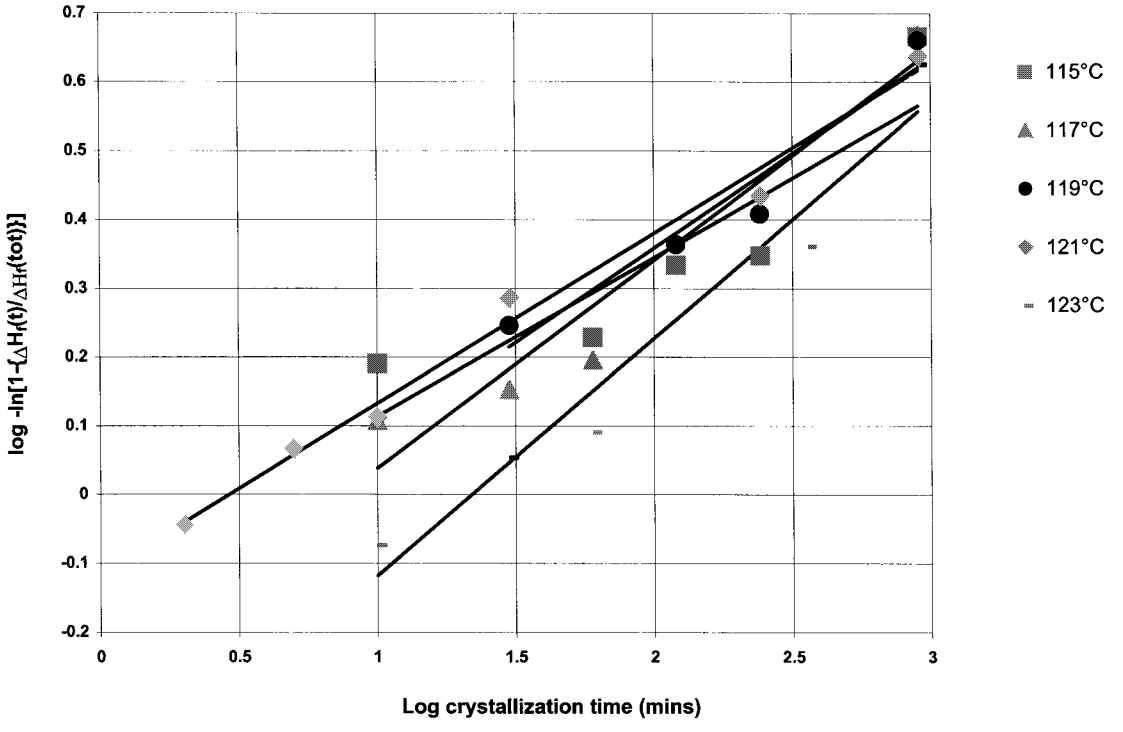

Fig. 7. Avrami plots (log $-\ln[1-\{\Delta H_f(t)/\Delta H_f(\text{tot})\}]$ versus logarithm of crystallisation time) for polymer A. The straight lines through the data set represents the best lines of fit using the method of least squares.

crystallisation processes after 40 s at a crystallisation temperature of 110°C.

Fig. 7 shows the results of Avrami analysis from melting data of a chromium catalysed polyethylene, polymer A. Avrami values and rate constants were similar to those of Fig. 6 with maximum crystallinity values around 35%, at the lowest crystallisation temperature. Measured differences in the Avrami plots were distinguished at higher temperatures of isothermal crystallisation. The Avrami exponents increased with increasing crystallisation temperature and rate constants correspondingly decreased. Low Avrami exponents were observed with values similar to those found in [6].

3.5. Non-isothermal crystallisation kinetics

Polymer B was the focus for non-isothermal crystallisation kinetic experiments. Fig. 8 shows the effect of cooling rate on the crystallisation of polymer B. Dual crystallisation peaks are evident. The first peak shows a moderate shift to lower temperatures as the cooling rate increases from 1°C/min to 80°C/min. The second peak, at approximately 65–70°C shifts even less. Fig. 9 shows these melting curves following all three cooling rates are very similar.

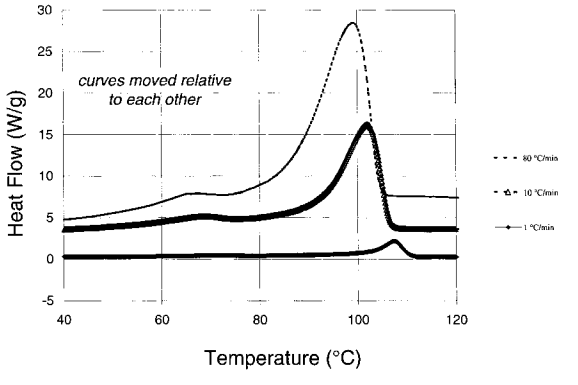

Fig. 8. Non-isothermal crystallisation curves for polymer B at different cooling rates (1°C/min to 80°C/min).

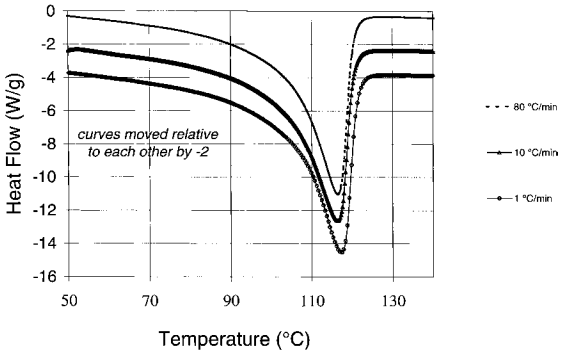

Fig. 9. Re-melting of crystallised samples of Fig. 8 (10°C/min). Curves are shifted for clarity.

3.6. Equilibrium melting temperature

It is useful to consider what the equilibrium melting of these materials might be by using the Hoffman–Weeks equation [7]. Eq. (2) based solely on thermodynamic principles makes no allowance for surface structure or topology. This equation relates melting temperature (T_m) to crystallisation temperature (T_c) as

$$T_m = T_c/\gamma + T_m^0 - T_m^0/\gamma, \quad (2)$$

where T_m^0 is the equilibrium melting temperature of a parallel infinite crystallite, and γ is the potential for lamellar thickening, a parameter that describes how far crystals are from their equilibrium state.

The equilibrium melting temperatures for both polymer A and polymer C are identical (141.5°C) and their respective γ values are slightly different (1.8 and 2.2 for polymers A and C, respectively) (see Fig. 10) [3,4]. The slopes of these curves denoted by γ provides a measure of the polymer's ability to thicken lamellar. Results show that this potential is greatest for polymer C (γ=2.2) followed by polymer A (γ=1.8). Polymer B shows an extraordinary isothermal crystallisation temperature versus melting point dependence. The extrapolated line over the steepest part of the curve shows a near parallel behaviour to the T_m=T_c line making the determination of the equilibrium melting temperature impossible. In addition, the lower temperature crystallisation region from 110°C to 90°C produces a near constant melting temperature in the range 115–117°C.

3.7. Modulated temperature differential scanning calorimetry

Fig. 11(a), (b), (c) and (d) shows results observed for polymer B on heating following crystallisation for 1 h and cooling at variable rates to room temperature from two extreme crystallisation temperature limits; 90°C and 115°C. Using the modulation conditions shown, we were able to achieve a minimum of 5–6 cycles through the melting transition. The maximum dynamic heating rate for this set of values is approximately 6.3°C/min and the minimum is zero.

The results of Fig. 11 are contrasted with those obtained from conventional non-modulated DSC experiments under similar crystallisation conditions. Fig. 11(a) shows MT-DSC traces of isothermal crystallisation at 90°C. In the non-reversing heat flow signal, exothermic activity coincides with melting processes observed in the reversing heat flow signal. The integrated areas under both peaks were different. In the non-reversing heat flow signal, the measured heat of crystallisation was −45 J/g and in the reversing heat flow signal, the heat of fusion was 160 J/g. These values were significantly different from the observed non-modulated heat flow signal (117 J/g) at the same underlying heating rate of 1°C/min. This value should equal the sum of the reversing and non-reversing heat flow. Fig. 11(b) shows results for the same experiment now cooled much more quickly, we obtained slightly higher values for the three signals under consideration. The integrated enthalpies were 170, −49 and 122 J/g for the reversing, non-reversing and conventional heat flow signals, respectively and the balance is sustained. Although the overall values were slightly higher in the rapidly cooled specimen, this difference was at most 3% of the weight fraction crystallinity. These results are within acceptable margins for error.

Crystallisation data at 115°C gives a different set of results. Both slow (Fig. 11(c)) and rapid (Fig. 11(d)) cooling give two melting endotherms. The earlier crystallisation experiments without cooling prior to re-melting gave only one main melting peak (Fig. 2). It is interesting to note that while the presence of a second melting peak is more distinct for high temperature crystallisation, the relative enthalpic contributions from the non-reversing and the reversing heat flow signals act to compensate the value from the non-modulated heat flow signal. The integrated enthalpies

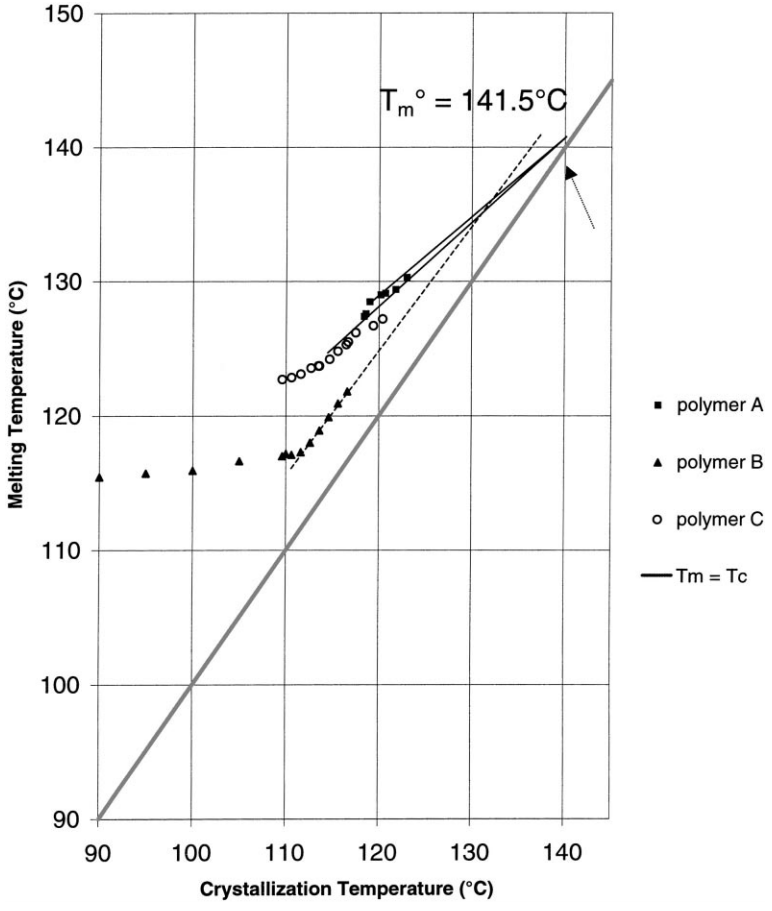

Fig. 10. Relationship between melting temperature and isothermal crystallisation temperature for polymers A, B and C. The extrapolation based on Eq. (2) forecasts an equilibrium melting temperature of 141.5°C and lamellar thickening parameters of 1.8 and 2.2 for polymers A and C, respectively. The equilibrium melting temperature of polymer B cannot be evaluated using this thermodynamic approach to melting.

of fusion in Fig. 11(c) were 211, −24 and 197 J/g for the reversing, non-reversing and non-modulated heat flow signals, respectively. Similarly, the integrated heat flows for Fig. 11(d) were 176, −36 and 146 J/g for the reversing, non-reversing and non-modulated heat flow signals, respectively. In contrast to the experiments conducted at 90°C, isothermal crystallisation at 115°C generated higher enthalpic contributions particularly from samples that had been cooled slowly following crystallisation. We presume this is a direct result of allowing more time for better crystal development on cooling.

Fig. 12 highlights the classic case where the application of MT-DSC has been employed to good effect in establishing initial crystallinities. The results are for polymer B. The melting endotherms indicate convincingly that initial crystallinities developed under isothermal conditions are indeed measurable. Fig. 12 shows melting endotherms following isothermal crystallisation at 115°C for 60 min without cooling after isothermal crystallisation from standard DSC and MT-DSC. The top curve (labelled total heat flow signal) represents the melting trace from conventional DSC whereas the bottom curve (labelled reversing heat flow signal) shows a similar melting trace under identical crystallisation conditions using temperature modulation and the reversing heat flow signal is shown. The integrated enthalpies were 50 J/g for the former and 56 J/g for the latter. These results translate to a 2% difference in weight fraction crystallinity in favour of

the reversing heat flow signal from MT-DSC. The difference, which manifests itself in the form of an exothermic crystallisation peak, is observed in the non-reversing heat flow signal (not shown here because of its small size). This result demonstrates that the total heat flow from conventional DSC is a weighted average of the combined signals from MT-DSC, i.e. reversing and non-reversing heat flow signals. However, melting and reorganisation are kinetic processes and thus the observed transition temperatures are not the same.

In attempting to study fractional crystallisation through molecular segregation effects we looked at quasi-isothermal crystallisation experiments as a guide to examining different metastable states within polymer lamellar microstructures. Fig. 13(a) shows schematically the procedure adopted to evaluate fractional crystallisation: cooling in 5°C steps with 5 min

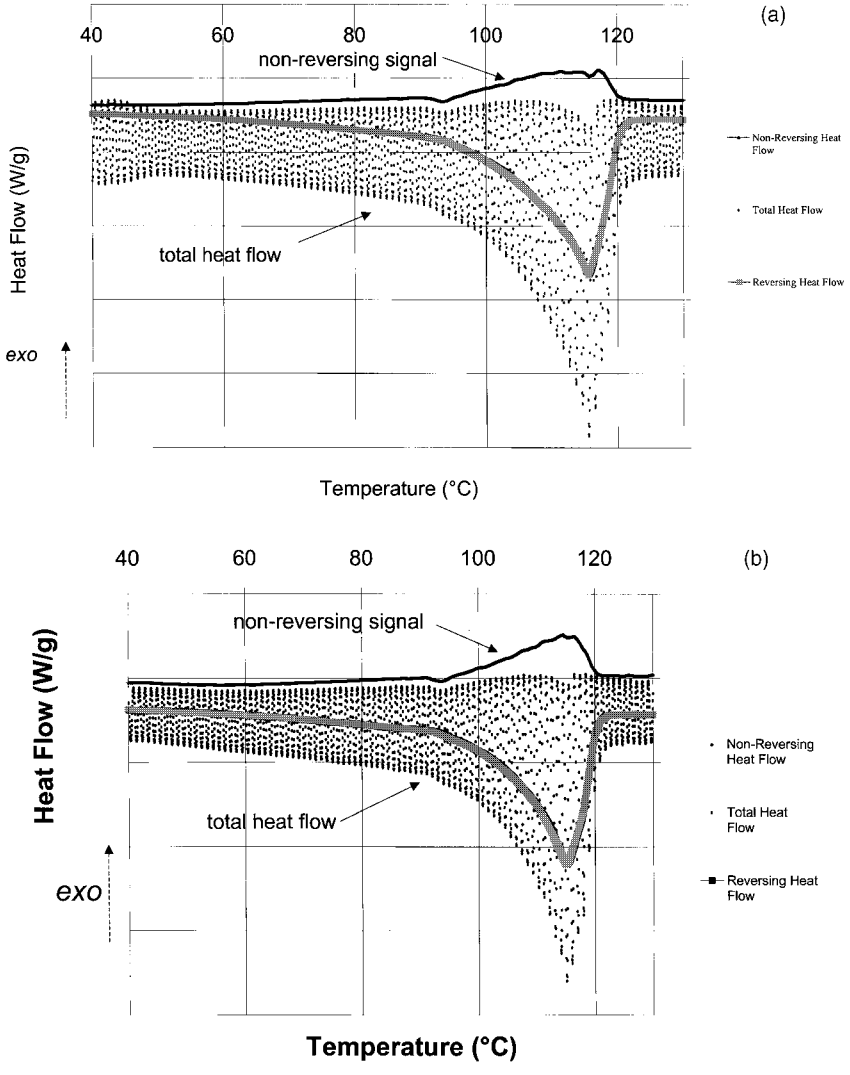

Fig. 11. Modulated temperature DSC traces on heating of polymer B crystallised at 90°C and 115°C following both rapid and slow cooling back down to room temperature. Modulation conditions were: 0.159°C amplitude, 60 s period and an average underlying heating rate of 1°C/min; (a) represents the heating trace of a specimen crystallised for 1 h at 90°C and cooled at ca. 1°C/min to room temperature; (b) as (a) but cooled at ca. 80°C/min. Figures (c) and (d): as (a) and (b) but crystallisation at 115°C.

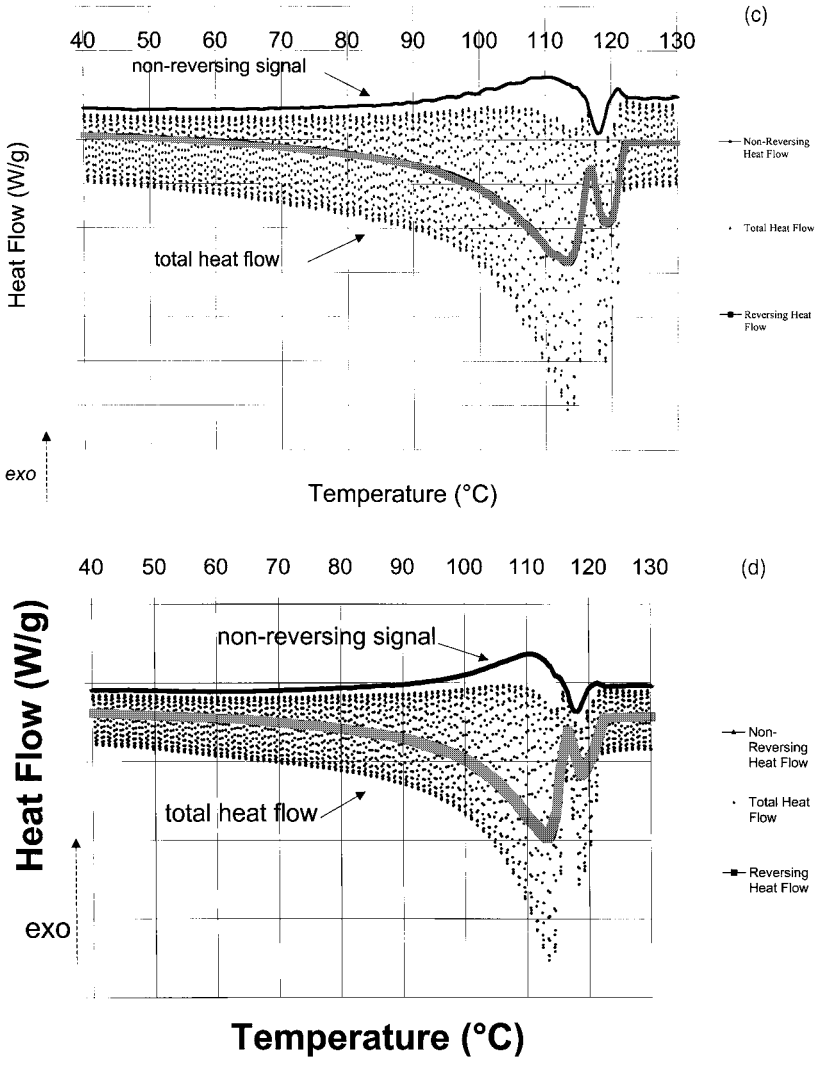

Fig. 11. (*Continued*)

isothermal periods followed by reheating at an average underlying modulated heating rate of 1°C/min with a temperature modulation of 0.159°C, using the ''heat-only'' mode in MT-DSC, i.e. no negative heating rates in the alternating cycle. Fig. 13(b) shows actual results from this type of sequential crystallisation experiment. Multiple melting endotherms were found to partially overlap with each other forming a continuous spectrum of melting histories. For this system, no detectable exothermic activity was found in the non-reversing heat flow signal. Melting of specimens prepared via step-wise crystallisation resulted in synchronous melting with both the non-reversing and reversing heat flow signals acting in-phase.

4. Discussion

From Table 1, it is clear that our polymers have similar densities despite significant differences in short chain branching, polydispersity and melting temperature. These differences relate to the different catalysts systems used for polymerisation. It is clear from Fig. 1 that polymer B has a broader melting

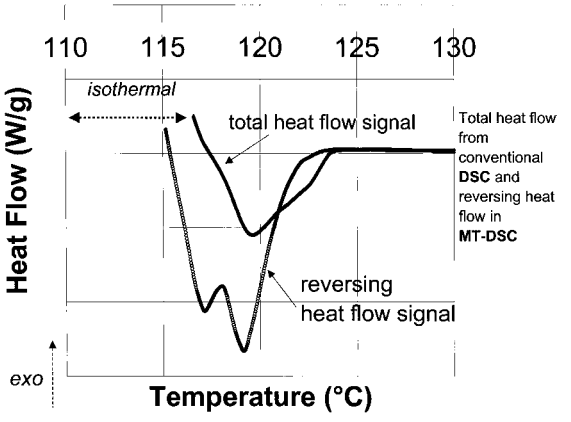

Fig. 12. Assessing initial crystallinities of polymer B using MT-DSC. The melting endotherms were recorded following isothermal crystallisation at 115°C for 60 min. The top curve shows the melting trace using conventional standard DSC at a heating rate of 1°C/min. The bottom curve shows the reversing heat flow signal from MT-DSC, with an underlying modulated heating rate of 1°C/min.

range than polymer A. The latter, chromium catalysed, polyethylene has a comparatively narrower and higher temperature melting range despite having the highest polydispersity.

In quantifying the relative rates of crystallisation from melting data, we have used Avrami analysis and results show rapid changes in crystallinity for lower temperatures of crystallisation followed by a period of slow growth. This rate of levelling out in crystallinity increases as a function of temperature. By contrast, the maximum degree of crystallinity, 33%, is achieved at the lower crystallisation temperatures compared with that found at the highest crystallisation temperature examined (115°C), 20%. In both cases, these values are much lower than the initial crystallinity values of the as-received materials (see Table 1) but slightly greater than values obtained directly from isothermal crystallisation kinetics.

Melting curves after isothermal crystallisation (see Fig. 2) show how the change in crystallinity develops with time. Fig. 2 suggests that there are two time dependent processes taking place, one of which is more sensitive to crystallisation temperature. At low crystallisation temperatures the principal contribution to the overall heat of fusion is derived from the ''upper'' melting peak. Although this melting endotherm develops with time and temperature, its counterpart the ''lower'' melting peak develops at a greater pace achieving prominence at 110°C. At 115°C, however, we suggest that the structure which leads to this lower temperature-melting peak, is thermodynamically unstable and cannot therefore be formed at this ''higher'' temperature. Loss of this structural form therefore accounts in part for the reduction in the overall heat of fusion (and crystallinity) with increasing crystallisation temperature. The Gaussian curves of Fig. 3, although having little scientific foundation, are helpful in visualising the magnitude of potential melting fractions.

The relative strengths of using either melting curves to infer crystallisation kinetics may be judged by comparison of the crystallisation behaviour of polymers B and C in Fig. 5 with that in Fig. 6. From Fig. 5, rapid crystallisation processes can be monitored by recording the crystallisation exotherm. The development of a second structure forming process, seen in Fig. 4(b)Fig. 5 with a local minimum in growth rate, marks the transition from one type of crystal growth to another. For best results in the development of crystallinity in relation to internal structure, long-time measurements are a convenient indicator of the state of this transformation; these longer-term results are consolidated in Figs. 6 and 7. Data from both techniques (melting kinetics versus crystallisation kinetics) are consistent at long times since comparable rate constants and similar Avrami exponents were obtained. This last point is demonstrated clearly in Fig. 14 using crystallinity data as opposed to heat of fusion data. This plot shows crystal fraction versus crystallisation time data for polymer B at 110°C obtained from both isothermal crystallisation and from melting behaviour following crystallisation. A dashed line is shown passing through both sets of data in a continuous manner. The isothermal crystallisation data at short times merge smoothly with melting data at long crystallisation times. This complementary use of crystallisation and melting kinetic data are extremely useful in describing the overall development of crystallinity over an extended time frame because each technique alone does not show the complete evolution of crystallinity.

Of particular interest is the time at which a transition between the different crystal growth phases occurs. Initial exploratory optical microscopy work suggests that this corresponds to the time for spheru-

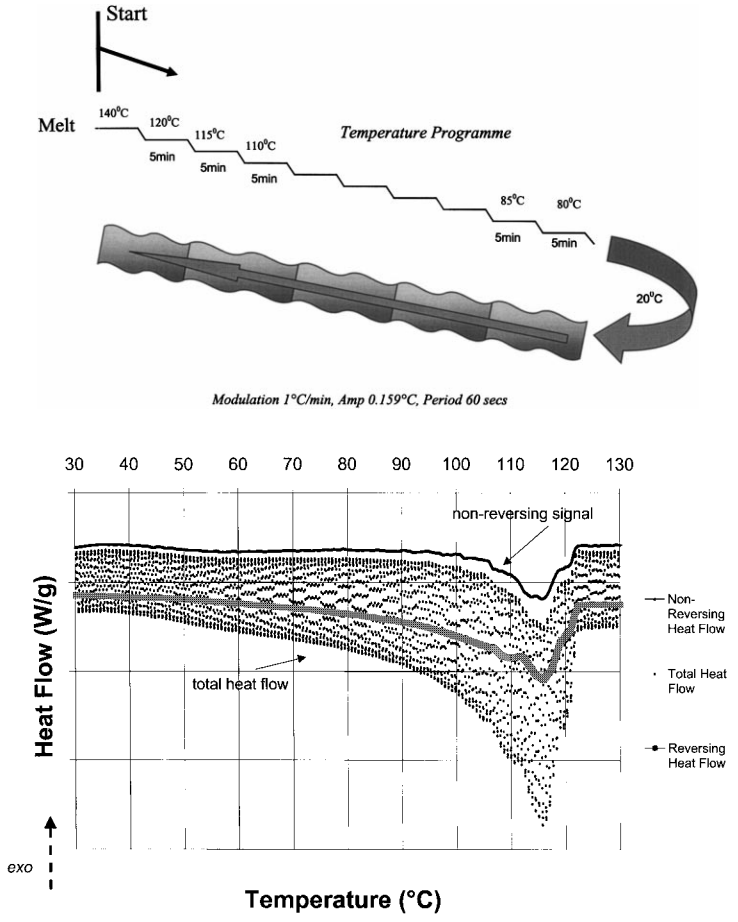

Fig. 13. Fractional stepwise crystallisation experiments from the melt: (a) schematic representation of the protocol adopted; (b) results obtained from this type of quasi-isothermal experiment from both conventional DSC and modulated temperature DSC.

litic or domain impingement. In addition, we suggest that, at impingement, there is a change in the crystallisation kinetics. Related work on low molar mass isotactic polypropylene fractions has shown this to be the case [8]. This would seem to indicate that the secondary crystallisation process, associated with the lower Avrami exponent, proceeds on a finer textural scale between first growth phase lamellae; these lamellae will stop growing at impingement and crystallisation will proceed in unoccupied regions between lamellae and at impingement boundaries.

From Fig. 6 some general trends are apparent: high temperature growth leads to greater Avrami exponents with smaller Avrami exponents at lower crystallisation temperatures. Similarly, rate constants, k, decreased from 10 to 2.5 for the temperature range of interest. In principle, we can determine the nucleation rate constants from knowledge of the spherulitic growth rates obtained from polarised light optical microscopy. This is, however, difficult as the spherulites and domains are small in most of the materials studied.

Comparing Fig. 7 with Fig. 6 it is apparent that polymer B has a much larger crystallisation temperature range (90–115°C) than polymer A (115–123°C). Growth at temperatures on either side of these ranges was either extremely fast or much too slow for accurate measurements.

Non-isothermal crystallisation experiments of polymer B showed that two crystallisation peaks occurred upon cooling. It was found that at the lower cooling rates the appearance of the second crystallisation peak was small and almost negligible, whereas at the high-

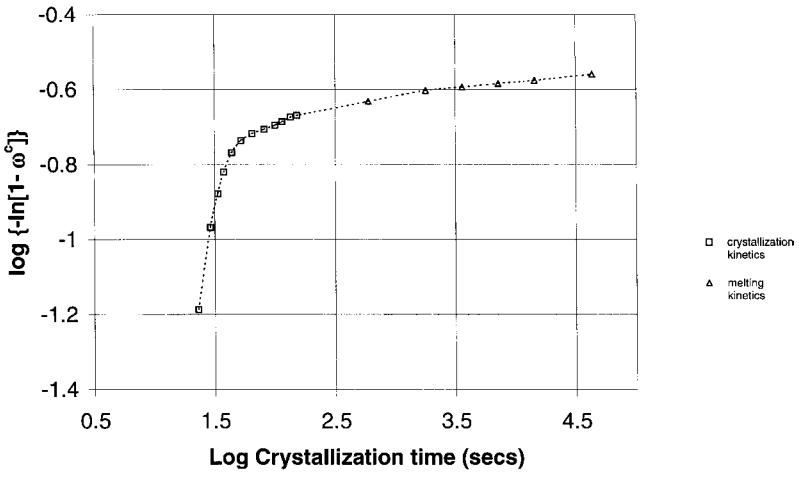

Fig. 14. A plot of log $\{-\ln[1-\omega^c]\}$ versus logarithm of crystallisation time (s) taken from Figs. 5 and 6 for polymer B crystallised isothermally at 110°C. The data is shown normalised to 293 J/g and is represented in classical Avrami format. The curved line through the data set is an interpolation of the complementary effect of crystallisation and melting kinetics data (see text). The open squares represent the data from isothermal crystallisation and the open triangles data from melting curves.

est rate investigated this second peak was significant. The cooling rate of −80°C/min is comparable to a number of commercially relevant cooling rates for film production. It is interesting to note that while distinct changes occurred upon cooling, very little if any change was seen upon heating (see Fig. 9) since each melting trace is superimposed on each other.

The equilibrium melting temperature of a polymer lamellar crystal is a very important thermodynamic quantity. The T_m versus T_c results (Fig. 10) show that results for polymers A and C can be extrapolated to the expected equilibrium melting temperature of 141.5°C. Polymer B on the other hand has results which run parallel to the $T_m=T_c$ line. This unusual behaviour would imply that simple thermodynamic considerations with respect to chain folded lamellar crystals are invalid and cannot be used here. Alamo et al. [9] have reported similar findings based on hydrogenated polybutadienes with fixed comonomer. Though no proof was provided, the authors tentatively suggested that the initial crystal size does not appreciably thicken with temperature, at least for samples prepared with low crystallinities. The limitation on lamellar thickness is thought to occur because polymer chains are prevented from escaping into the lamellar interfacial region and are thus unable to chain extend on heating. Small angle X-ray scattering (SAXS), in combination with DSC, has shown that in linear polyethylenes without SCB, lamellar thickening readily occurs with SAXS curves showing a maximum that moves to small angles. However, heating branched polyethylenes with significant levels of SCB and branch lengths greater than butyl the Bragg maximum in the SAXS curve changes very little.

From the MT-DSC results of Fig. 11(a) and (b), separation of a second melting endotherm in polymer B appears evident while development of a dual melting peak in the reversing heat flow signal is seen most clearly at the highest temperatures of crystallisation, namely 115°C, with strong evidence for reorganisation processes occurring throughout the crystallisation range examined. Crystallisation at 115°C (Fig. 11(c) and (d) our highest investigated crystallisation temperature) reveals that, following slow cooling (−1°C/min), a large upper temperature melting peak occurs in the reversing heat flow signal. At more rapid rates of cooling (−80°C/min) the lower melting peak curve is more pronounced. Interpretation of the melting curves revealed enthalpies generally in line with the results obtained from isothermal crystallisation experiments in the same temperature range (when making allowances for the different scanning rates). The usual explanation offered in interpreting dual melting behaviour is based on rates of crystallisation. Usually, slow rates of crystallisation lead to large-scale molecular segregation and more perfect crystals, which have

higher melting temperatures. What we have observed here is broadly in line with this. Crystallisation at 115°C demonstrates this effect by the appearance of two distinct melting peaks. The effects of molecular segregation are in theory reduced at lower temperatures of crystallisation, however, molecular segregation occurs on a much finer scale. Discrimination of the various populations of crystals is therefore not so evident (see Fig. 11(a) and (b)) with melting displaying only one broad peak.

Confirmation that MT-DSC can evaluate the initial crystallinity state of semicrystalline polymers has already been established [10,11]. Its application in determining initial crystallinities is demonstrated here in Fig. 12. The top curve from conventional DSC (total heat flow signal) is contrasted with the bottom curve from MT-DSC (reversing heat flow signal) that provides direct evidence for crystal reorganisation processes on thermal scanning. Reorganisation (top curve) is manifested in this particular example by higher transition temperatures for both melting endotherms. Interestingly enough, the reversing heat flow signal shows a 2% increase in crystallinity over that observed in the total heat flow signal. This increase, offset by small exothermic increases in the non-reversing heat flow signal, provides evidence for crystallisation occurring in parallel with melting. Consequently, the magnitude of the total heat flow signal masks subtle reorganisational processes that take place during thermal scanning.

Evaluation of fractional crystallisation behaviour in a series of high temperature stepwise crystallisation experiments from the melt (see Fig. 13) was undertaken to attempt to promote segregation and remove reorganisational effects [12,13]. We observed multiple melting endotherms superimposed on the main melting temperature from 105°C and above. In stark contrast to the results of Figs. 11 and 12, we observed no reorganisation activity in the non-reversing heat flow signal; rather discrete melting was observed in the reversing heat flow signal [14]. We believe this follows as a consequence of negligible reorganisation through re-crystallisation during melting. Cooling in a controlled and step-wise manner produced fully crystallised crystal populations limited by the physical constraints of a pre-defined lamellar thickness. Consequently, very little material is available to anneal and reorganise on rescanning. The results thus show sequential melting of specific populations of crystals having well-defined morphologies which have been stabilised during each isothermal crystallisation step. An alternative view is that the kinetics of reorganisation at each isothermal step is sufficiently rapid that near-stable crystals are formed. On subsequent rescanning the potential for reorganisation is significantly reduced or absent.

5. Conclusions

Polymers A and C have identical equilibrium melting temperatures, however, polymer B which crystallises a few degrees below its melting temperature cannot be evaluated in the same way. Crystallisation at low temperatures did not show significant evidence for molecular segregation and reorganisational effects. Low Avrami exponents were observed from the melting kinetics study while typical Avrami exponents for the initial crystallisation is distinguishable from lamellar thickening processes that can be observed at longer times. We suggest that the transition between these two extremes of kinetics is marked by spherulitic (or domain) impingement. We have also shown that MT-DSC is able to separate reorganisational from melting processes and step-wise crystallisation is capable of removing reorganisational contributions to the DSC response.

Acknowledgements

We gratefully acknowledge the support of Fina Research, Feluy (Belgium).

References

[1] W.O. Statton, P.H. Geil, J. Appl. Polym. Sci. 3 (1960) 357.
[2] D.C. Bassett, Principles of Polymer Morphology, Cambridge University Press, Cambridge, 1981.
[3] B. Wunderlich, Macromolecular Physics, vol. 3, Crystal Melting, Academic Press, New York, 1980.
[4] J.D. Hoffman, G.T. Davis, J.I. Lauritzen Jr, in: N.B. Hannay (Ed.), Treatise on Solid State Chemistry, vol. 3, Chapter 7, Plenum Press, New York, 1976.
[5] M. Avrami, J. Chem. Phys. 7 (1939) 1103, idem 8 (1940) 212.

[6] E. Martuscelli, M. Pracella, G.D. Volpe, P. Greco, Makromol. Chem. 185 (1984) 1041.
[7] J.D. Hoffman, J.J. Weeks, J. Chem. Phys. 37 (1962) 1723.
[8] J.J. Janimak, S.Z.D. Cheng, Polym. Bull. 22 (1989) 95.
[9] R.G. Alamo, E.K.M. Chan, L. Mandelkern, I.G. Voigt-Martin, Macromolecules 25 (1992) 6381.
[10] M. Reading, D. Elliott, V.L. Hill, J. Therm. Anal. 40 (1993) 949.
[11] A. Toda, T. Oda, M. Hikosaka, Y. Saruyama, Thermochim. Acta 293 (1997) 47.
[12] M. Guo, Q. Fu, S.Z.D. Cheng, Polymer Reprints 38(2) (1997).
[13] S.Z.D. Cheng, Private Communication, 1998.
[14] Internal Report, Polymer Research Centre, University of Surrey, 1998: Report number PRC03/98/FINA.